

# Evidence for unconventional superconductivity in a spinel oxide

Huanyi Xue<sup>1,\*</sup>, Lijie Wang<sup>1,\*</sup>, Zhongjie Wang<sup>1,\*</sup>, Guanqun Zhang<sup>1</sup>, Wei Peng<sup>2,3</sup>, Shiwei Wu<sup>1,4</sup>, Chunlei Gao<sup>1,4,†</sup>, Zhenghua An<sup>1,4,†</sup>, Yan Chen<sup>1</sup>, and Wei Li<sup>1,†</sup>

<sup>1</sup>*State Key Laboratory of Surface Physics and Department of Physics, Fudan University, Shanghai 200433, Peoples Republic of China*

<sup>2</sup>*State Key Laboratory of Functional Materials for Informatics, Shanghai Institute of Microsystem and Information Technology, and Center for Excellence in Superconducting Electronics, Chinese Academy of Sciences, Shanghai 200050, Peoples Republic of China*

<sup>3</sup>*Center of Materials Science and Optoelectronics Engineering, University of Chinese Academy of Sciences, Beijing 100049, Peoples Republic of China*

<sup>4</sup>*Institute for Nanoelectronic Devices and Quantum Computing, Fudan University, Shanghai 200433, Peoples Republic of China*

\*These authors contributed equally to this work

†Correspondence and requests for materials should be addressed to C.G. (email: [clgao@fudan.edu.cn](mailto:clgao@fudan.edu.cn)), Z.A. (email: [anzhenghua@fudan.edu.cn](mailto:anzhenghua@fudan.edu.cn)), and W.L. (email: [w\\_li@fudan.edu.cn](mailto:w_li@fudan.edu.cn)).

**The charge frustration with mixed-valence state inherent to  $\text{LiTi}_2\text{O}_4$  that is found to be a unique spinel oxide superconductor, is the impetus for special attentions to unveil the clues of the pairing mechanism in unconventional superconductivity. Here we report a pronounced in-plane fourfold rotational symmetry of the superconductivity in high-quality single crystalline  $\text{LiTi}_2\text{O}_4$  (001) thin films. Both the magnetoresistance and upper critical field under in-plane magnetic field manifest striking fourfold oscillations deep inside the superconducting state, and the anisotropy vanishes in the normal state, demonstrating that is intrinsic property of the superconducting phase. We attribute this behavior to the unconventional  $d$ -wave-like superconducting Cooper pairs in  $\text{LiTi}_2\text{O}_4$ , which is further supported by the scanning tunneling spectroscopy. Our findings demonstrate the unconventional character of the pairing interaction in three-dimensional spinel oxide superconductor and shed new light into understanding the pairing mechanism of unconventional superconductors.**

The appearance of intriguing superconductivity arises from Cooper pairing between conducting electrons, and one of the prominent issues about superconductivity is its pairing symmetry which provides a fundamental understanding of the Cooper pair formations in superconductivity<sup>1-4</sup>. In conventional superconductors, a condensate of Cooper pairs exhibits an isotropic  $s$ -wave pairing symmetry which is independent of directions over the entire Fermi surface<sup>5</sup>. In unconventional superconductors, the superconducting Cooper pairs have an anisotropic gap functions belonging to nontrivial representations of the crystal symmetry group which are not invariant under all symmetry elements<sup>1,2</sup>, such as the rotational symmetry breaking in layered two-dimensional copper oxide high  $T_c$  superconductors displaying an anisotropic  $d$ -wave pairing<sup>6-8</sup>. Notably, this rotational symmetry is spontaneously broken by strong Coulomb repulsion in strongly correlated electron system of cuprate that could lead to a novel many-body effect and give rise to Cooper pair states with orbital wave function with angular momentum greater than zero ( $s$ -wave)<sup>2,4</sup>.

Spinel oxides are another striking class of strongly correlated electron system that possesses charge frustration with mixed-valences and complicated interactions among charge, orbit, and spin induced by Jahn-Teller distortion, promoting many fascinating and appealing electronic phases. Among them, the charged frustrated lithium titanate ( $\text{LiTi}_2\text{O}_4$ ) with mixed-valences of  $\text{Ti}^{3+}: 3d^1$  and  $\text{Ti}^{4+}: 3d^0$  is a unique spinel oxide superconductor with  $T_c$  onset of 13 K<sup>9</sup>. In the past, specific heat measurements on a polycrystalline  $\text{LiTi}_2\text{O}_4$  suggest this system to be a candidate of Bardeen-Cooper-Schrieffer (BCS)-like conventional  $s$ -wave superconductor<sup>10</sup>. However, the non-negligible complex electron-electron correlations via spin-fluctuations in superconductivity have been extensively revealed in X-ray absorption and resonant inelastic soft X-ray scattering<sup>11,12</sup>, nuclear magnetic resonance<sup>13</sup>, and magnetic susceptibility measurements<sup>14</sup>. Renewed measurements on high-quality  $\text{LiTi}_2\text{O}_4$  thin films find an anomalous magnetoresistance in the normal state<sup>15</sup> and a pseudo-gap opening at the Fermi energy<sup>16</sup> through the electrical transport and scanning tunneling spectroscopy (STS), respectively, in recent years. These works imply  $\text{LiTi}_2\text{O}_4$  to be a possible unconventional and nontrivial superconductor driven by the intimate correlation between Cooper pairing and charge frustration associated with the strong spin-fluctuations. Here, in the present report, we revisit and discuss the possible pairing symmetry of the superconductivity in  $\text{LiTi}_2\text{O}_4$  (001) thin films by using both the angular resolved magnetoresistance and upper critical field, and find a pronounced in-plane fourfold rotational symmetry manifested deep inside the superconducting state, but vanished in the normal state. These results significantly demonstrate that the anisotropy with fourfold rotational symmetry is an intrinsic property of the superconducting phase in  $\text{LiTi}_2\text{O}_4$ , and thus we attribute the three-dimensional  $\text{LiTi}_2\text{O}_4$  to be a  $d$ -wave-like pairing unconventional superconductor. In addition, this  $d$ -wave-like pairing symmetry in  $\text{LiTi}_2\text{O}_4$  is further supported by the measurement of STS.

The high-quality single crystalline thin films of spinel  $\text{LiTi}_2\text{O}_4$  (001) are epitaxially grown on the  $\text{MgAl}_2\text{O}_4$  (001) ( $a_{\text{MAO}} = 0.8080$  nm) substrates by pulsed laser deposition. Bulk  $\text{LiTi}_2\text{O}_4$  is a face-centered-cubic (fcc) spinel structure at room-temperature with lattice parameter  $a = 0.8405$  nm<sup>9</sup> (Fig. 1a), consisting of the

tetrahedral and octahedral sites occupied by the lithium and titanium cations, respectively. The X-ray diffraction (XRD)  $2\theta$ -scan for the  $\text{LiTi}_2\text{O}_4$  thin films is measured (Fig. 1b), which displays clear (004) Bragg reflection peaks of films and substrates with the absence of additional peaks down to the sensitivity limit of the diffractometer, suggesting  $c$ -oriented growth of  $\text{LiTi}_2\text{O}_4$  thin film. The out-of-plane lattice parameter and the thickness of  $\text{LiTi}_2\text{O}_4$  thin films are estimated to 0.84 nm and 30.2 nm, respectively, deduced from the formula of Laue oscillation, in good agreement with that of bulk<sup>9</sup>. The  $\varphi$ -scan of the {404} diffraction planes displays fourfold rotational symmetry of crystal lattice at the same angular positions (Fig. 1c), implying in-plane ordering for thin film and substrate. In Fig. 1d the reciprocal space mapping of the (404) peak is carried out for further confirming the epitaxial growth as well. These measurements, including the large-area atomic force microscopy [Fig. S1 in supplementary information (SI)], demonstrate high-quality epitaxial growth of the  $\text{LiTi}_2\text{O}_4$  films on  $\text{MgAl}_2\text{O}_4$  substrates.

Figure 2a displays the temperature dependent longitudinal electrical resistance  $R_{xx}$  on the two representative as-growth  $\text{LiTi}_2\text{O}_4$  thin films (Sample #1 and #2) with the Hall bar structure, schematically illustrated in the inset of Fig. 2a. A typical metallic behavior at the normal state and a sharp superconducting transition at  $T_c$  (onset of 13 K for Sample #1 and 12 K for Sample #2) are clearly observed, with a narrow and sharp transition width of less than 0.5 K. Temperature dependent DC magnetization measurements with both field-cooling (FC) and zero-field-cooling (ZFC) modes under an applied out-of-plane magnetic field of 50 Oe are also carried out to further examine the superconductivity in  $\text{LiTi}_2\text{O}_4$  thin film (Sample #1), as shown in Fig. 2b. The observed negative magnetic susceptibility that is the ratio of the measured magnetization to the applied magnetic field, indicates the diamagnetism induced by the Meissner effect, unambiguously confirming the appearance of superconductivity below  $T_c$ . These results are highly reproducible and agree reasonably with previous electrical transport studies<sup>9,15</sup>. Furthermore, the magnetoresistance  $R_{xx}(\mu_0 H)$  (here,  $\mu_0$  is the vacuum permeability) with the fields perpendicular ( $\mu_0 H_{\perp}$ ) and parallel ( $\mu_0 H_{\parallel}$ ) to the sample plane surface of  $\text{LiTi}_2\text{O}_4$  thin film (Sample #2) are shown in Fig. 2c (Sample #1

in Fig. S2 of SI). The fundamental superconducting behaviors are clearly observed that the superconducting critical fields  $\mu_0 H_{c2}^{mid}$  [ $H_{c2,\parallel}^{mid}$  for parallel field along  $a(b)$ -axis and  $H_{c2,\perp}^{mid}$  for perpendicular field] shift parallel down to a lower value, where  $\mu_0 H_{c2}^{mid}$  are evaluated at the midpoints of the normal state resistance. This shift arises from the magnetic field induced orbital effect, which leads to the appearance of Abrikosov vortices and forms a regular array of vortex lines parallel to the magnetic field. As a result, the kinetic energy of superconducting currents around the vortex cores reduces the superconducting condensation energy<sup>17,18</sup>. Notably, both directions of magnetic field do not significantly affect the magnetoresistance, which suggests that  $\text{LiTi}_2\text{O}_4$  is a three-dimensional superconductor with an isotropic out-of-plane  $\mu_0 H_{c2}^{mid}$ . For a quantitative estimation, the superconducting upper critical fields  $\mu_0 H_{c2}^{mid}$  are plotted as a function of temperature, and the phase diagram of  $H_{c2}^{mid}$ - $T$  is shown in Fig. 2d. The Werthamer-Helfand-Hohenberg (WHH) model<sup>19</sup> is further used to fit the upper critical fields  $\mu_0 H_{c2}^{mid}$ . The extracted  $\mu_0 H_{c2}^{mid}$  at zero temperature limit is 18.3 T, and the superconducting coherence length  $\xi_{GL}(T = 0 \text{ K})$  is thus estimated from the Ginzburg-Landau formula<sup>17</sup>  $\mu_0 H_{c2}^{mid} = \frac{\Phi_0}{2\pi\xi_{GL}^2}$  with the fluxoid quantization  $\Phi_0$  as 4.2 nm, consistent with previous findings<sup>20,21</sup>.

Next, we turn to discuss the in-plane anisotropy of magnetoresistance on the  $\text{LiTi}_2\text{O}_4$  thin films with the Corbino disk geometry (Fig. 3a), which could eliminate the Lorentz force induced extrinsic anisotropy<sup>22,23</sup> when the in-plane magnetic field is rotated relative to the crystal axes. The  $\alpha$  is defined as an azimuthal angle between the magnetic field and the  $a(b)$ -axis of the lattice, as indicated in Fig. 3a. In the normal state ( $T = 30 \text{ K}$  in Fig. 3b), the magnetoresistance  $R_{xx}$  is found to be essentially independent of the in-plane azimuthal angle  $\alpha$ , displaying an isotropic behavior. This result is in a marked contrast to that twofold rotational symmetry in magnetoresistance in the normal state reported on the Hall bar structure in the previous experiment<sup>15</sup>, suggesting that the previously observed twofold rotational symmetry in the normal state is attributed to an extrinsic effect mainly originated from the Lorentz force (also see Fig. S3 in SI). In the superconducting state ( $T = 6.5 \text{ K}$  in Fig. 3b), we observe a pronounced fourfold

modulation of the magnetoresistance  $R_{xx}$  (Figs. 3b-e), which is consistent across multiple samples. In this case, the anisotropic magnetoresistance  $R_{xx}$  attains the maximum value when the magnetic field is directed to the  $[110]$  and  $[1,-1,0]$  orientations ( $\alpha = \pm 45^\circ$ ) and becomes minimum when the field is directed along the axis of the lattice ( $\alpha = 0^\circ$  and  $90^\circ$ ). Considering the fact that the existence of striking fourfold oscillations in magnetoresistance manifests deep inside the superconducting region, and vanishes in the normal state, we could straightforwardly rule out the possibilities of extrinsic contributions, such as the twin structure in the orthorhombic electronic phases<sup>24</sup> and the cubic band structure (see Fig. S5 and Fig. S6 in SI) inherent to the  $\text{LiTi}_2\text{O}_4$  crystal with respect to the underlying fourfold lattice symmetry shown in Fig. 1c, and thus demonstrate that the fourfold rotational symmetry is an intrinsic property of the superconducting phase in  $\text{LiTi}_2\text{O}_4$ .

To further reveal the fourfold symmetric behavior of superconductivity in  $\text{LiTi}_2\text{O}_4$  reflecting the superconducting gap structure, we extract the upper critical field  $\mu_0 H_{c2}$  from the in-plane azimuthal angle  $\alpha$  dependent magnetoresistance  $R_{xx}$  in the superconducting region. Due to the relatively larger values of the upper critical field  $H_{c2}$  than the strength of applicable magnetic field (see Fig. 2d), we alternatively redefine the points of zero value of magnetoresistance  $R_{xx}$ ,  $\mu_0 H_{c2}^{zero}$ , as shown in Fig. 4b and 4c. Interestingly, the in-plane  $\alpha$  dependent  $\mu_0 H_{c2}^{zero}$  also displays fourfold periodicity, providing another strong evidence for the fourfold rotational symmetry of the superconductivity in  $\text{LiTi}_2\text{O}_4$ . In addition, this oscillation of  $H_{c2}^{zero}$  has a  $\pi$  phase shift by comparing with that of the magnetoresistance  $R_{xx}$  shown in Fig. 3c, such that at the in-plane azimuthal angles  $\alpha$  where superconductivity is hardest to suppress,  $H_{c2}^{zero}$  is largest and the magnetoresistance  $R_{xx}$  is lowest (Fig. 3c and Fig. 4c), as expected from our intuitions<sup>25</sup>. Theoretically, it has been demonstrated that the in-plane fourfold symmetric  $H_{c2}^{zero}$  could be resulted from a  $d$ -wave pairing symmetry<sup>24</sup>. Therefore, the fourfold symmetry in  $H_{c2}^{zero}$  inherent to the superconducting Cooper pairs enables us to specify the existence of node directions. Since the  $H_{c2}^{zero}$  takes maxima for the magnetic field applied parallel to the lattice axes, and minima for the directions rotated  $45^\circ$  relative to the axes, the superconducting gap leads to be maximum along the lattice

axes and minimum along the [110] and [1,-1,0] directions ( $\alpha = \pm 45^\circ$ ), signaling that the pairing symmetry of the three-dimensional  $\text{LiTi}_2\text{O}_4$  most likely belongs to the  $d_{x^2-y^2}$ -like-wave associated with the nodes along the directions of minima of  $H_{c2}^{zero}$  (see Fig. 4a). In fact, a clear fourfold modulation of  $H_{c2}$  in the superconducting state with an applied in-plane magnetic field which reflects the angular position of nodes of  $d_{x^2-y^2}$ -wave symmetry has also been observed in cuprates with two-dimensional layered Cu-O planes<sup>26,27</sup>.

At last, the measurement of STS is also carried out to further examine the superconducting gap features. Fig. 4d displays a typical tunneling conductance ( $dI/dV$ ) spectrum as a function of an applied bias voltage ( $V_s$ ) at the surface of  $\text{LiTi}_2\text{O}_4$  thin films with fixed temperature of 4.2 K. Notably, the tunneling conductance with sharp coherence peaks does not go to zero at the Fermi energy and a pronounced V-shaped-like behavior rather than the U-shaped one is clearly visible, suggestive of the existence of superconducting gap with nodes having gapless excitations in  $\text{LiTi}_2\text{O}_4$ . In addition, the theoretical models with both the  $s$ -wave and  $d_{x^2-y^2}$ -wave pairing are fitted to the superconducting gap quantitatively using the Dynes formula<sup>28,29</sup>. Through the theoretically fitting shown in Fig. 4d, we find that the theoretical curve of  $d$ -wave pairing well reproduces the STS spectrum, and the fitted superconducting gap  $2\Delta_g$  is 4.8 meV. This result provides the further evidence for the  $d$ -wave-like pairing superconductivity in  $\text{LiTi}_2\text{O}_4$ , indicative of an unconventional superconducting pairing mechanism, such as the anisotropic spin-fluctuations induced by the charge frustration with mixed-valence state of  $\text{Ti}^{3.5+}$  inherent to  $\text{LiTi}_2\text{O}_4$ . Therefore, the anisotropic  $d$ -wave-like Cooper pairs hosted in the spinel oxide  $\text{LiTi}_2\text{O}_4$  with three-dimensional superconductivity is an intriguing example followed by the high- $T_c$  cuprates with two-dimensional superconductivity, which not only opens a new platform to clarify the emergence of unconventional superconductivity with a delicate interplay of charge frustration associated with spin-fluctuations and the Cooper pairs, but also dawns the revised theories for the pairing mechanism of the unconventional superconductivity.

## Materials and Methods

**Thin films growth and structural characterization.** The spinel  $\text{LiTi}_2\text{O}_4$  (001) thin films are epitaxially grown on  $\text{MgAl}_2\text{O}_4$  (001) substrates ( $4 \times 4 \times 0.5 \text{ mm}^3$ ) by pulsed laser deposition in an ultrahigh-vacuum chamber (base pressure of  $10^{-8}$  Torr). Prior to growth, the  $\text{MgAl}_2\text{O}_4$  substrates are annealed at  $800 \text{ }^\circ\text{C}$  for 2 hours in air, to obtain a smooth surface (Fig. S1 in SI). During deposition, the sintered  $\text{Li}_4\text{Ti}_5\text{O}_{12}$  ceramic target (Kurt J. Lesker Company) is used to grow the  $\text{LiTi}_2\text{O}_4$  films with a KrF excimer laser (Coherent 102, wavelength:  $\lambda = 248 \text{ nm}$ ). A pulse energy of 110 mJ and a repetition rate of 10 Hz are used. The  $\text{LiTi}_2\text{O}_4$  films are deposited at  $750 \text{ }^\circ\text{C}$  in a vacuum chamber to promote growth of the superconducting phase. All the samples are cooled to room temperature at a constant rate of  $20 \text{ }^\circ\text{C}/\text{min}$  in vacuum after deposition. The crystalline quality and epitaxy relationship of  $\text{LiTi}_2\text{O}_4$  thin films are examined by four-circle XRD (Bruker D8 Discover, Cu  $K\alpha$  radiation,  $\lambda = 0.15406 \text{ nm}$ ) operated with high-resolution mode using a three-bounce symmetric Ge (022) crystal monochromator.

**Magnetization and electrical transport measurements.** Before electrical transport measurements, the magnetic properties of the  $\text{LiTi}_2\text{O}_4$  films are measured using a superconducting quantum interference devices (SQUID) magnetometer (MPMS, Quantum Design Inc.). For measurement of the direct current (DC) magnetization as a function of temperature, the samples are first cooled to 2 K in zero field, and then an out-of-plane magnetic field of 50 Oe is applied. The magnetization data are collected during warming from 2 K to 30 K (ZFC process). In the same fixed field, the samples are then cooled to 2 K again, and the magnetization data are recollected during warming from 2 K to 30 K (FC process). The electrical transport measurements are performed using in a cryostat (Oxford Instruments TeslatronPT cryostat system). The Hall bar structure (inset of Fig. 2a) and Corbino<sup>23</sup> (Fig. 3a) are fabricated by ion-beam etching to measure the electrical transport properties.

**Scanning tunneling spectroscopy measurements.** The features of superconducting gap on  $\text{LiTi}_2\text{O}_4$  thin films are measured using STS cooled by liquid Helium. The tunneling conductance ( $dI/dV$ ) spectrum as a function of an applied bias voltage ( $V_s$ ) at the surface of  $\text{LiTi}_2\text{O}_4$  thin films with fixed temperature of 4.2 K, which is measured with the assistance of a lock-in amplifier, and the bias modulation applied is  $\Delta U_{rms} = 200 \text{ } \mu\text{V}$  ( $f = 983 \text{ Hz}$ ) and the tip-sample distance is set by  $U = 10 \text{ mV}$ ,  $I = 100 \text{ pA}$ . The single band Dynes formula<sup>28,29</sup> with the pairing formation of  $s$ -wave and  $d$ -wave are used for fitting the tunneling conductance ( $dI/dV$ ).

## References

1. Sigrist, M. & Ueda, K. Phenomenological theory of unconventional superconductivity. *Rev. Mod. Phys.* **63**, 239 (1991).
2. Tsuei, C. C. & Kirtley, J. R. Pairing symmetry in cuprate superconductors. *Rev. Mod. Phys.* **72**, 969 (2000).
3. Norman, M. R. The challenge of unconventional superconductivity. *Science* **332**, 196-200 (2011).
4. Stewart, G. R. Unconventional superconductivity. *Adv. in Phys.* **66**, 75-196 (2017).
5. Bardeen, J., Cooper, L. N., & Schrieffer, J. R. Theory of Superconductivity. *Phys. Rev.* **108**, 1175 (1957).
6. Shen, Z.-X. *et al.* Anomalously large gap anisotropy in the *a-b* plane of  $\text{Bi}_2\text{Sr}_2\text{CaCu}_2\text{O}_{8+\delta}$ . *Phys. Rev. Lett.* **70**, 1553 (1993).
7. Tsuei, C. C. *et al.* Pairing symmetry and flux quantization in a tricrystal superconducting ring of  $\text{YBa}_2\text{Cu}_3\text{O}_{7-\delta}$ . *Phys. Rev. Lett.* **73**, 593 (1994).
8. Wu, J. *et al.* Spontaneous breaking of rotational symmetry in copper oxide superconductors. *Nature* **547**, 432–435 (2017).
9. Johnston, D. C. *et al.* High temperature superconductivity in the Li-Ti-O ternary system. *Mater. Res. Bull.* **8**, 777-784 (1973).
10. McCallum, R. W. *et al.* Superconducting and normal state properties of  $\text{Li}_{1+x}\text{Ti}_{2-x}\text{O}_4$  spinel compounds. II. Low-temperature heat capacity. *J. Low Temp. Phys.* **25**, 177–193 (1976).
11. Durmeyer, O. *et al.* Ti K XANES in superconducting  $\text{LiTi}_2\text{O}_4$  and related compounds. *J. Phys.: Condens. Matter* **2**, 6127-6136 (1990).
12. Chen, C. L. *et al.* Role of 3d electrons in the rapid suppression of superconductivity in the dilute V doped spinel superconductor  $\text{LiTi}_2\text{O}_4$ . *Supercond. Sci. Technol.* **24**, 115007 (2011).
13. Tunstall, D. P. *et al.* Titanium nuclear magnetic resonance in metallic superconducting lithium titanate and its lithium-substituted derivatives  $\text{Li}_{1+x}\text{Ti}_{2-x}\text{O}_4$  ( $0 < x < 0.10$ ). *Phys. Rev. B* **50**, 16541 (1994).
14. Johnston, D. C. Superconducting and normal state properties of  $\text{Li}_{1+x}\text{Ti}_{2-x}\text{O}_4$  spinel compounds. I. Preparation, crystallography, superconducting properties, electrical resistivity, dielectric behavior, and magnetic susceptibility. *J. Low Temp. Phys.* **25**, 145–175 (1976).
15. Jin, K. *et al.* Anomalous magnetoresistance in the spinel superconductor  $\text{LiTi}_2\text{O}_4$ . *Nature Communications* **6**, 7183 (2015).
16. Okada, Y. *et al.* Scanning tunnelling spectroscopy of superconductivity on surfaces of  $\text{LiTi}_2\text{O}_4$  (111) thin films. *Nature Communications* **8**, 15975 (2017).
17. Tinkham, M. Introduction to Superconductivity, 2nd edn (McGraw-Hill, New York, 1996).
18. Jiang, D. *et al.* Strong in-plane magnetic field induced reemergent superconductivity in the

van der Waals heterointerface of NbSe<sub>2</sub> and CrCl<sub>3</sub>. *ACS Applied Materials & Interfaces* **12**, 49252 (2020).

19. Werthamer, N. R., Helfand, E., & Hohenberg, P. C. Temperature and purity dependence of the superconducting critical field, H<sub>c2</sub>. III. Electron spin and spin-orbit Effects. *Phys. Rev.* **147**, 295 (1966).

20. Wei, Z. *et al.* Anomalies of upper critical field in the spinel superconductor LiTi<sub>2</sub>O<sub>4-δ</sub>. *Phys. Rev. B* **100**, 184509 (2019).

21. Chopdekar, R. V. *et al.* Growth and characterization of superconducting spinel oxide LiTi<sub>2</sub>O<sub>4</sub> thin films. *Physica C* **469**, 1885-1891 (2009).

22. Paltiel, Y. *et al.* Instabilities and disorder-driven first-order transition of the vortex lattice. *Phys. Rev. Lett.* **17**, 3712-3715 (2000).

23. Li, J. *et al.* Nematic superconducting state in iron pnictide superconductors. *Nature Communications* **8**, 1880 (2017).

24. Takanaka, K. & Kuboya, K. Anisotropy of upper critical field and pairing symmetry. *Phys. Rev. Lett.* **75**, 323 (1995).

25. Hamill, A. *et al.* Two-fold symmetric superconductivity in few-layer NbSe<sub>2</sub>. *Nature Physics* **17**, 949-954 (2021).

26. Hanaguri, T. *et al.* Anisotropy of upper critical field in the (110)<sub>t</sub> and (001)<sub>t</sub> planes for single-crystal La<sub>1.86</sub>Sr<sub>0.14</sub>CuO<sub>4</sub>. *Physica B* **165&166**, 1449 (1990).

27. Koike, Y. *et al.* Fourfold symmetry in the *ab* plane of the upper critical field for single-crystal Pb<sub>2</sub>Sr<sub>2</sub>Y<sub>0.62</sub>Ca<sub>0.38</sub>Cu<sub>3</sub>O<sub>8</sub>: Evidence for *d<sub>x<sup>2</sup>-y<sup>2</sup></sub>* pairing in a high-*T<sub>c</sub>* superconductor. *Phys. Rev. B* **54**, R776(R) (1996).

28. Dynes, R. C., Narayanamurti, V. & Garno, J. P. Direct measurement of quasiparticle-lifetime broadening in a strong-coupled superconductor. *Phys. Rev. Lett.* **41**, 1509 (1978).

29. Machida, T., Kohsaka, Y. & Hanaguri, T. A scanning tunnelling microscope for spectroscopic imaging below 90 mK in magnetic fields up to 17.5 T. *Rev. Sci. Instrum.* **89**, 093707 (2018).

## Acknowledgments

This work was supported by the National Natural Science Foundation of China (Grant Nos. 11927807 and 12027805) and Shanghai Science and Technology Committee (Grant Nos. 19ZR1402600 and 20DZ1100604).

## Author contributions

W.L. conceived the project and designed the experiments. H.X. grew the samples. L.W. and W.P. performed the XRD measurements. L.W. performed the electrical transport and magnetization measurements. H.X. and Z.A. did the sample nano-fabrications. Z.W. and C.G. performed the STS measurements. W.L. wrote the paper. All authors discussed the results and gave approval to the final version of the manuscript.

## **Author Information**

**The authors declare no competing financial interests.** Correspondence and requests for materials should be addressed to C.G. (email: [clgao@fudan.edu.cn](mailto:clgao@fudan.edu.cn)), Z.A. (email: [anzhenghua@fudan.edu.cn](mailto:anzhenghua@fudan.edu.cn)), and W.L. (email: [w\\_li@fudan.edu.cn](mailto:w_li@fudan.edu.cn)).

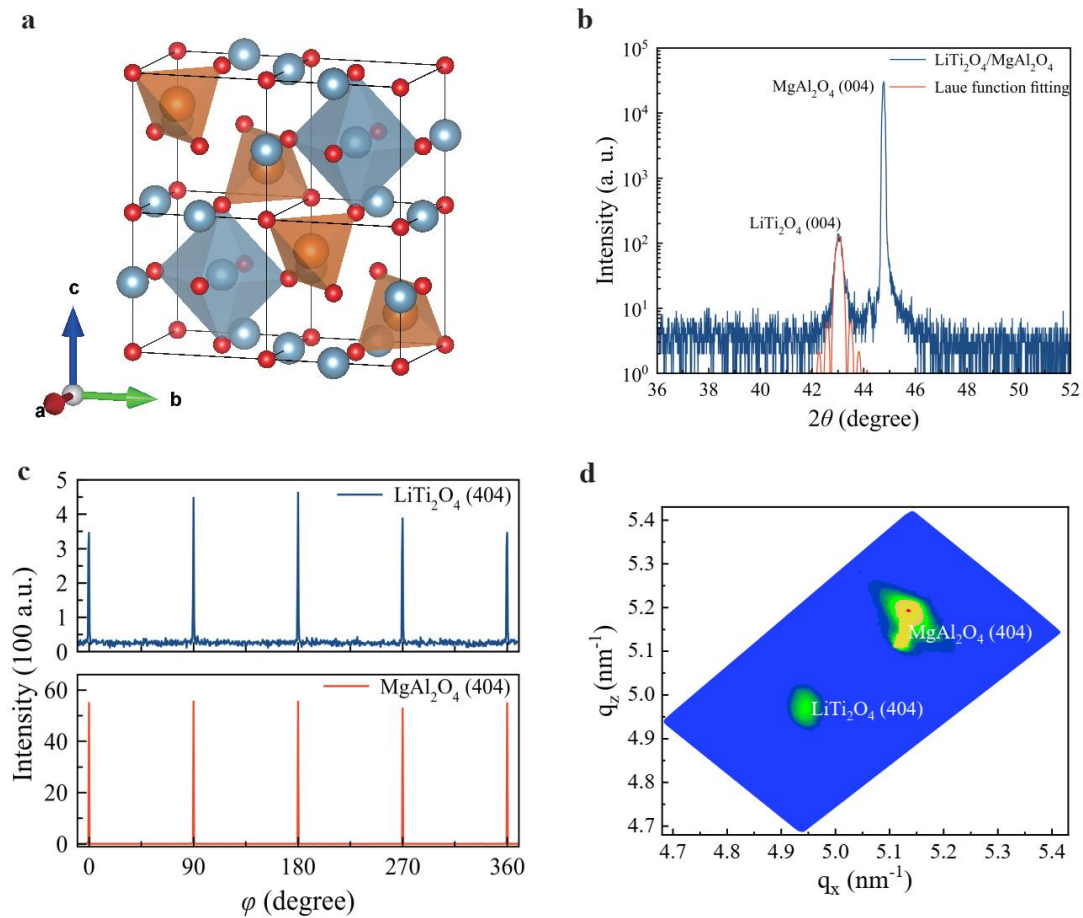


**Fig. 1. The structural characteristics of  $\text{LiTi}_2\text{O}_4$ .** **a**, Schematic illustration of crystal structure for spinel oxide  $\text{LiTi}_2\text{O}_4$ . **b**,  $2\theta$  XRD spectra of the epitaxial  $\text{LiTi}_2\text{O}_4$  (001) thin films grown on  $\text{MgAl}_2\text{O}_4$  (001) substrate. The Laue function fitting is shown in (b). **c**,  $\varphi$ -scan of the {404} diffraction planes for the  $\text{LiTi}_2\text{O}_4$  thin film and  $\text{MgAl}_2\text{O}_4$  substrate. Four peaks are uniformly distributed to display in-plane fourfold rotational symmetry of lattice, implying the in-plane epitaxy. **d**, Reciprocal space mapping of (404) peaks for both the thin film and substrate.

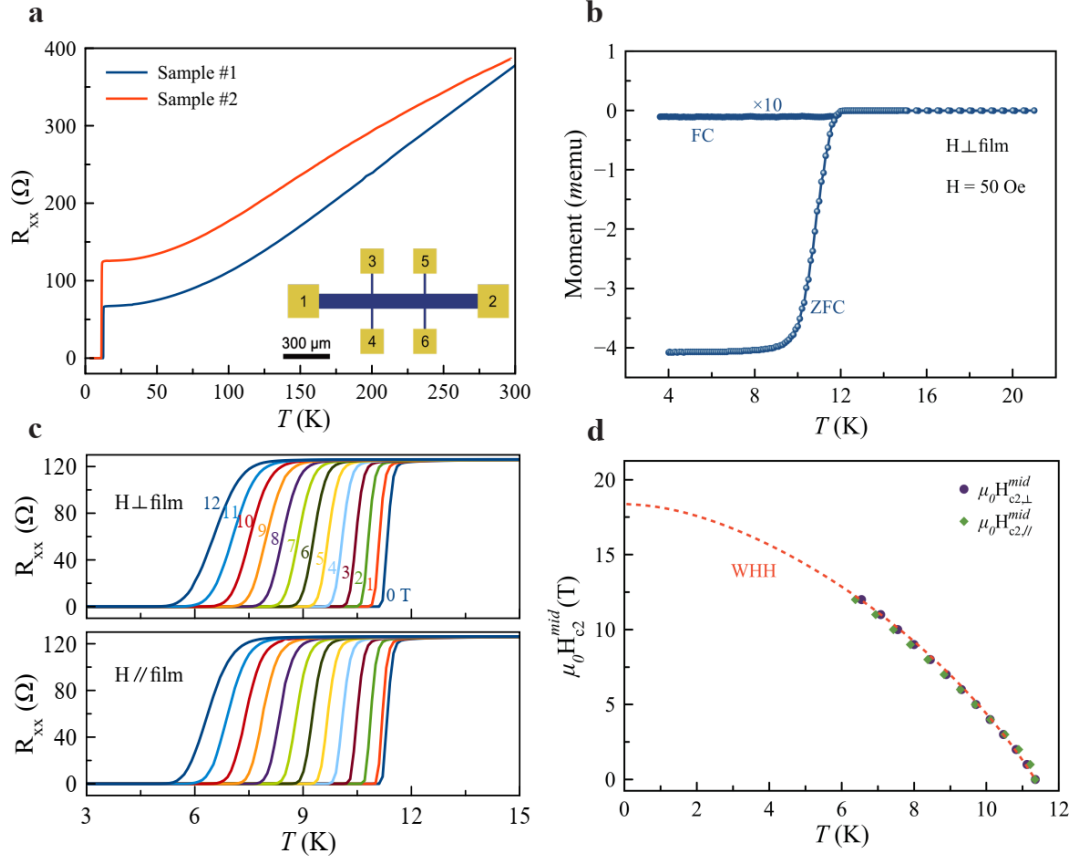


**Fig. 2. The superconducting properties of  $\text{LiTi}_2\text{O}_4$  (001) thin films.** **a**, Longitudinal electrical resistance ( $R_{xx}$ ) as a function of temperature ranging from 2 K to 300 K at zero magnetic field for two representative  $\text{LiTi}_2\text{O}_4$  (001) thin films (Sample #1 and #2). The Hall bar structure is schematically illustrated in the inset of (a). **b**, Temperature dependent DC magnetization of  $\text{LiTi}_2\text{O}_4$  (001) thin film (Sample #1) in FC and ZFC modes with an applied out-of-plane magnetic field of 50 Oe. We note that the FC values in (b) are scaled by a factor of 10. **c**, Magnetoresistance for fields perpendicular and parallel to the sample plane surface of Sample #2. **d**, The Corresponding temperature dependence of upper critical fields  $\mu_0 H_{c2}^{mid}$  [ $H_{c2,\parallel}^{mid}$  for in-plane field along  $a(b)$ -axis and  $H_{c2,\perp}^{mid}$  for our-of-plane field], which are determined at the half of values of  $R_{xx}$  in (c). The red dashed line is fitted by WHH theory.

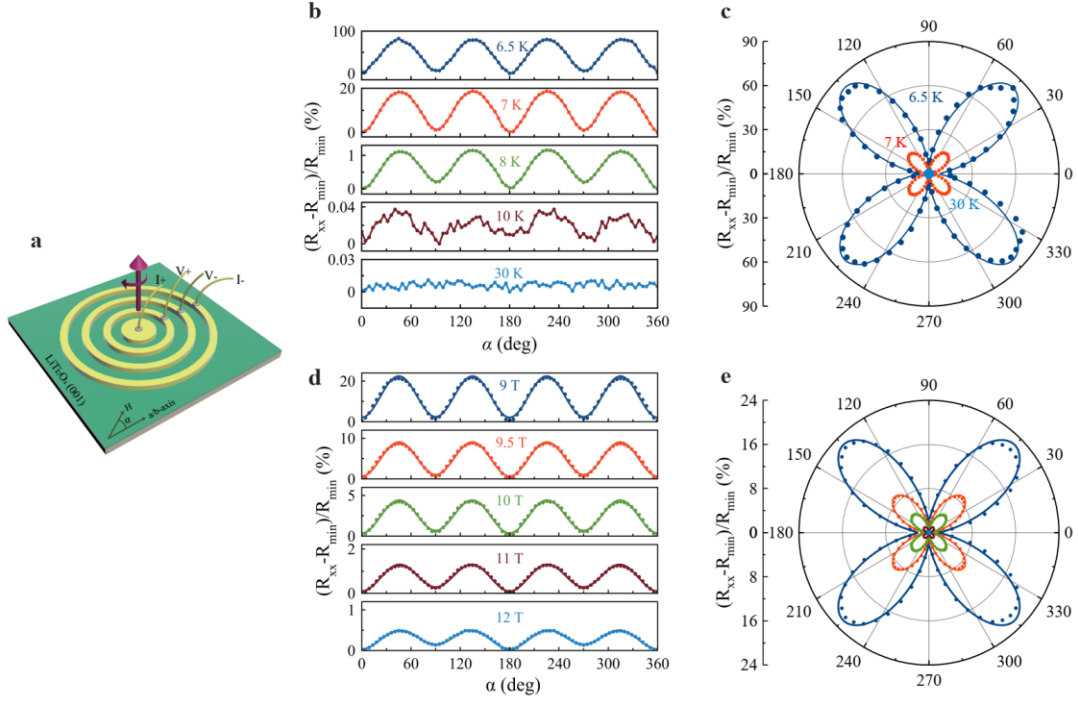


**Fig. 3. Magnetoconductance signature of fourfold superconducting behavior in  $\text{LiTi}_2\text{O}_4$  (001) thin films.** **a**, Schematic image of the Corbino-shape device for angular-dependent in-plane magnetoconductance ( $R_{xx}$ ) measurements. The angle  $\alpha$  is set to zero ( $\alpha = 0$ ) when the field is applied parallel to one of  $a(b)$ -axis. **b**, Angular dependent ratio of magnetoconductance  $R_{xx}$ , normalized by minimum value of  $R_{xx}$  ( $R_{\min}$ ), at various temperatures for the applied magnetic field of 12 T. **c**, Polar plots of the data in (b). **d**, Field dependent ( $T = 8$  K) ratio of magnetoconductance  $R_{xx}$ , normalized by minimum value of  $R_{xx}$  ( $R_{\min}$ ). **e**, Polar plot of the data in (d).

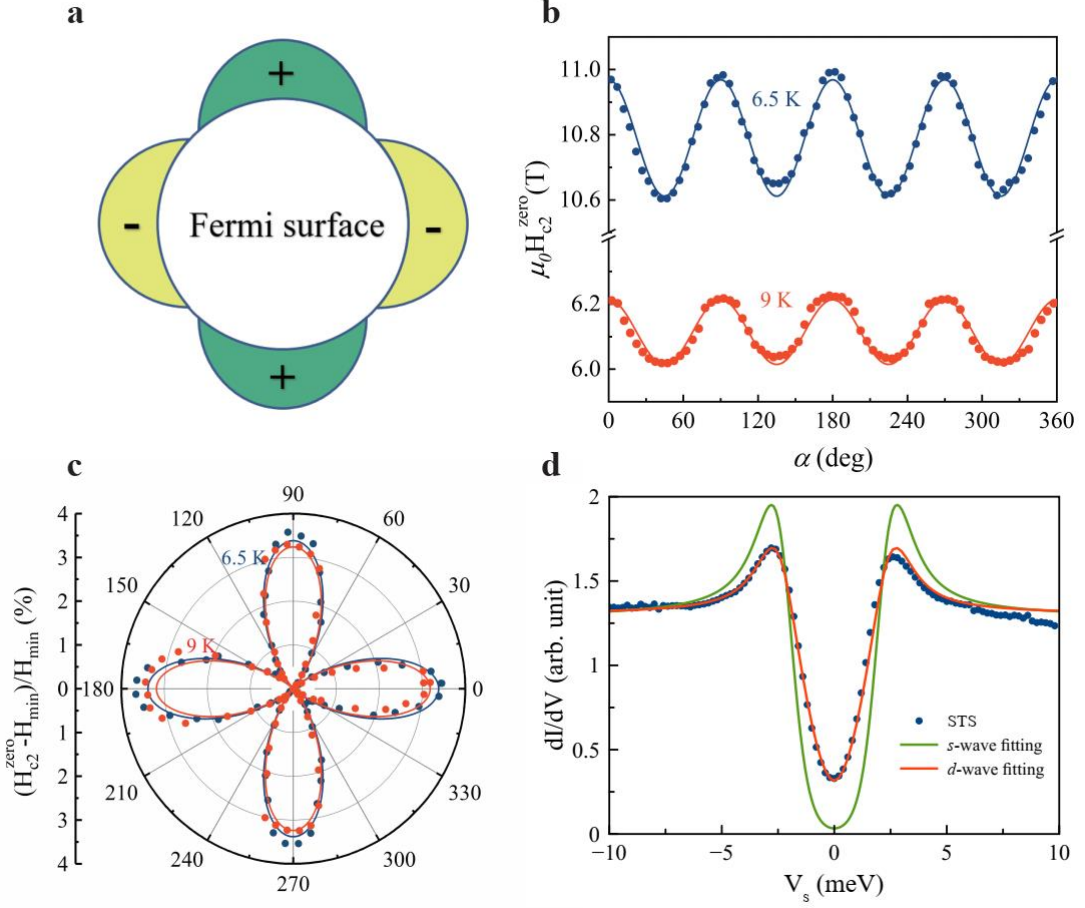


**Fig. 4.** *d*-wave-like pairing signature of LiTi<sub>2</sub>O<sub>4</sub> (001) thin films. **a**, Schematics of the  $d_{x^2-y^2}$ -wave superconducting gaps on the Fermi surface. **b**, In-plane angular dependent  $\mu_0 H_{c2}^{zero}$  at various temperatures. Here  $H_{c2}^{zero}$  is extracted at the points of zero value of magnetoresistance  $R_{xx}$  shown in Fig. 3b. **c**, Polar plots of the normalized data by minimum value of  $H_{c2}^{zero}$  ( $H_{min}$ ) in (b). **d**, High-resolution tunneling conductance spectrum ( $dI/dV$ ,  $2\Delta_g = 4.8$  meV) on the surface of LiTi<sub>2</sub>O<sub>4</sub> at 4.2 K by using STS. The *s*-wave and *d*-wave fitting curves are also shown in (d), indicating that the superconducting gap symmetry of LiTi<sub>2</sub>O<sub>4</sub> is a *d*-wave-like pairing.